A Decoupled Control Scheme of Four-Port Solid State Transformer

Saban Ozdemir[1,3], Necmi Altin[1,2], Ahmad El Shafei[1], Mo Rashidi[4], and Adel Nasiri[1]

[1] Center for Sustainable Electrical Energy Systems, University of Wisconsin-Milwaukee, WI, USA
[2] Department of Electrical and Electronics Engineering, Faculty of Technology, Gazi University, Ankara, Turkey
[3] Department of Energy Systems Engineering, Faculty of Technology, Gazi University, Ankara, Turkey
[4] Eaton Corporation, Menomonee Falls, WI, USA
nasiri@uwm.edu; www.uwm.edu/sees

***Abstract*— In this study, a four-port solid-state transformer (SST) with decoupled control scheme to control the power flow and the output voltage is proposed. The proposed decoupled control scheme controls all of the four ports' powers independently. In addition, the design of the four-port transformer including core material selection and winding placement is investigated. The designed transformer is modeled in ANSYS-Maxwell and also co-simulated with ANSYS-Simplorer. The operating frequency of the system is designed for 100 kHz; therefore, a very compact size is obtained for the entire multi-port converter. The performance of the proposed system is validated throughout MATLAB/Simulink simulation and experimental studies carried out for a 10kW/port SST prototype. The obtained results show that the four-port SST provides an interface for four-different power supplies or loads. It is seen that the proposed decoupled control scheme can control the output voltage at the desired value and track the reference power signals for each port. It provides as well a good steady state and dynamic performance.**

Keywords—multi-port transformer, four-port transformer, decoupled control, solid state transformer, power flow control.

I. INTRODUCTION

The solid state transformer (SST) is a combination of power electronic converter and high or medium-frequency transformer that connects two voltage zones. In addition to the normal functionalities of the conventional transformers, such as galvanic isolation and voltage matching, the SST benefits the power distribution system by enabling active power and voltage control, real time monitoring and control of its ports [1]-[4]. Due to the medium or high-frequency operation of the transformer, the size is much smaller than a conventional low frequency transformer (LFT) for the same voltage and power ratings. This size and weight reduction is a key motivation for designing high-frequency SSTs and isolated power electronic converters.

Recent studies have shown the importance of local installation of energy storage units, like battery energy storage systems, as one of the main requirements for the future architecture of the distribution system for supporting local demands. This provides many advantages in terms of reliability, resiliency, and power quality. However, independent power converters are required to operate with battery energy storage systems. Similarly, when photovoltaic (PV), battery energy storage and/or fuel cells systems are employed in a micro-grid or local power system, several two-port DC-DC converters are adopted to control and manage the system [5], [6]. This requirement decreases both power density and reliability [7]. Similar issues are valid for the electrical vehicle applications. Battery supported fuel cell vehicles or super-capacitor applications require multiple DC-DC converters. Although in some studies converters are designed as a multi-port structure to transfer energy to each other via a common DC bus, the requirement of electrical isolation between ports was not satisfied. Also, the conversion ratio between the ports in some cases are very high, and thus, these structures cannot be used. These requirements lead to the use of several isolated two-port DC-DC converters [6] and as a result, multiple transformers employed in the system will lead to a decrease in power density and reliability, and to an increase in the total cost [7].

Multi-port converters have been discussed and used for different applications including: thetraction (electrical trains) applications [8],[9], the electrical vehicle power distribution systems [10], and the hybrid distributed generation (DG) applications [7]. Multi-port solid state transformer or multi-port isolated converter topology is an extension version of the Dual Active Bridge (DAB) converter that uses common transformer core for power sharing instead of common DC bus. Multi-port SSTs (MPSSTs) are investigated to improve the overall power density, cost and reliability [7]-[11]. The power of the MPSST flowing from one port to another is controlled by the phase-shift angle between these two ports. However, the other ports are affected as well in this phase shifting action; their corresponding phase-shift angles have to be changed in order to keep their power/voltage levels at the desired values. It is seen that increasing the number of ports also increases the control complexity of the converter. Therefore, galvanic isolated MPSSTs has been widely proposed for three-port systems [12]-[14]. A suggested topology of three-phase three-port systems was discussed in [15]. A limited number of control schemes have been suggested for MPSSTs. In [12], an open loop power sharing control scheme is introduced for three-port MPSST. This approach is based on the natural power sharing characteristics of a galvanically isolated three-port resonant DC-DC converter. However, only a sample operation mode (two ports are transferring power to the third one) is considered. In addition, non-ideal conditions like parameter mismatch and/or voltage fluctuations are not considered. A control scheme based on switch turn-on time is proposed for a flyback transformer based three-port MPSST [13]. However, this controller scheme is only designed for flyback

transformer-based systems, and it is not discussed in much details. There are limited number of studies on controlling four-port SST [7]. Since power flow and voltage regulation are overly complicated by the increase in the number of ports, the controller design is a challenge for these converters. Therefore, a decoupled control scheme is an important requirement to control the power of each port.

In this paper, a four-port SST topology is developed to be used as a compact integration node for a distribution system with four voltage zones; DG, battery energy storage system, grid, and a load as shown in Fig. 1. A four-port MPSST and a

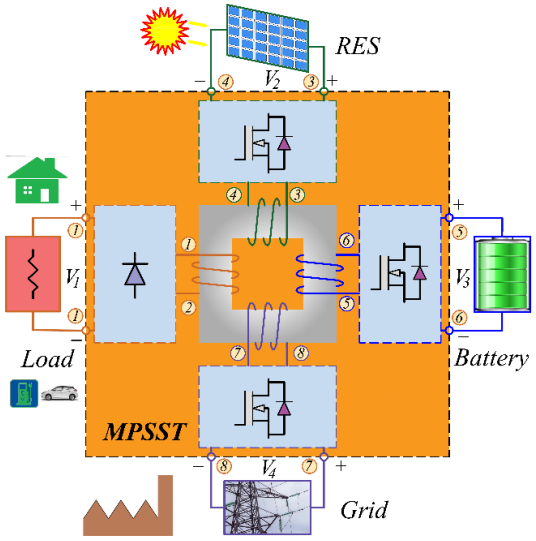

Fig. 1. Four-port MPSST configuration.

decoupled control scheme is presented to control the output voltage and port power levels. There are three active converters interconnecting the grid, the energy storage, and the DG source. These devices could be in a different combination depending on the application in hand. The active switch-based converters are full-bridge single-phase converters enabling bidirectional power flow for grid and energy storage ports. The same converter is used for the unidirectional power conversion on the DG port. Finally, the load is connected to the fourth port. Due to the non-generating nature of the load, a unidirectional single-phase diode bridge rectifier is used for this port. It is assumed that an energy management system is employed which determines the power references for all ports. Then, each active converter is controlled to track these reference signals. The operation of the proposed system is validated with MATLAB/Simulink simulations and experimental studies performed on a 10 kW/port MPSST prototype. Simulation and experimental results have confirmed that the proposed control method is suitable for multi-port solid state transformer systems in terms of quality measures such as steady state and dynamic response.

II. Four-Port High Frequency Transformer Design

Transformer design is one of the most important processes in SST design. In order to build an optimal transformer, some design parameters such as core material, cross sectional area, volume, shape, winding configuration, number of turns, wire type, maximum flux density, leakage and magnetizing inductances, parasitic capacitance between the four windings, core and winding losses and the efficiency of the transformer should be analyzed. Considering parameters such as size, energy density, etc., the operating frequency is selected to be 100 kHz.

As it is known, four core materials which are mainly silicon steel, amorphous, nanocrystalline and ferrite are used in medium and high frequency transformer design. In Fig. 2, these four different core materials are compared in terms of flux density, price, operating frequency and loss. Although the silicon steel provides higher saturation flux density values, its loss characteristics limit its use in high frequency applications.

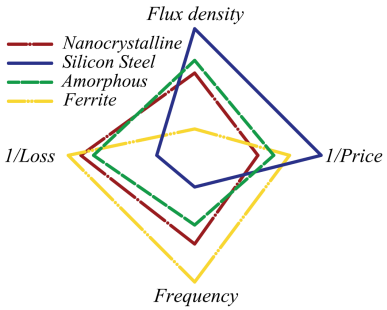

Fig. 2. Comparing different core materials for HF transformer

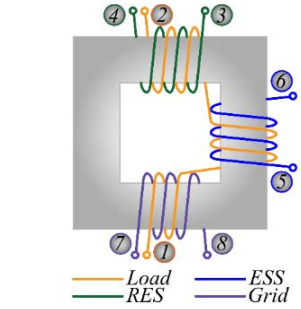

(a)

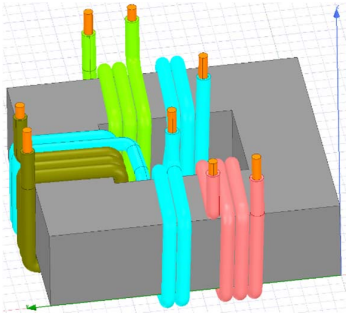

(b)

Fig. 3. a) Selected core and coupling style b) ANSYS-Maxwell-3D model

Today, using silicon steel may be suitable up to a few kHz operating frequency. As for the case of Amorphous and Nanocrystalline core materials; their saturation flux density is lower than silicon steel but higher than the ferrite. Therefore, they offer smaller core size and can provide more compact design. However, higher operating frequency conditions, like 100kHz as the case in this study, the increase in core losses is more dominant over the decrease in the core size being compared to ferrite [1], [3] [16]. As a result, 3C94 ferrite core was selected to be the most suitable material for our application.

Another important parameter to be looked after is the leakage inductance. It directly affects the efficiency and power transfer capability of the power converters. While higher leakage inductance values limit the power transfer capability and causes a decrease in efficiency, it also limits the peak value of the transformer current. Therefore, an optimal value should be determined to achieve the design objectives. In multi-port solid state transformer design, different winding placement also effects many parameters such as wire resistance, leakage and magnetization inductances, leakage capacitance of the windings, etc. After conducting extensive and thorough design studies, it is seen that in terms of leakage inductance and wire length, the winding placement given in Fig. 3(a) provides better results. Then, this design is modelled in a Finite Element Analysis (FEA) analysis tool (ANSYS-Maxwell) as shown in Fig. 3(b).

Transient and Electrostatic simulations have been done through ANSYS-Maxwell, and then a co-simulation (ANSYS-Maxwell and ANYSY-Simplorer simulating the model together) of the model is performed. The flux distribution obtained from transient simulation studies is given in Fig. 4. As it is seen from the figure, there is no saturation, so maximum flux density target is achieved. The voltage waveforms obtained from the co-simulation studies are given in Fig. 5. As a result of these studies, transformer parameters are obtained as given in Table 1. Then the designed transformer is implemented and the prototype of the transformer is shown in Fig. 6.

III. A Decoupled Control System Design for Four-Port SST

In this study, a four port SST control scheme is designed. The control of four-port SST is very similar to the control of a dual-active bridge (DAB) converter. Therefore, the equation for power delivered from port-x to port-y can be written as follows:

$$P_{xy} = \frac{V_x' V_y'}{2\pi^2 f_s L_{xy}} \phi_{xy}(\pi - \phi_{xy}) \quad ;\phi_{xy} = \phi_x - \phi_y \qquad (1)$$

where P_{xy} is the power transferred from port-x to port-y; ϕ_x and ϕ_y are phase shift angles of the converters port-x and port-y, respectively; V_x' and V_y' are DC voltages referred to the AC side of port-x and port-y, respectively; f_s is the switching frequency, and L_{xy} is the equivalent inductance between port-x and port-y.

TABLE I. The MPSST Design Details

Parameter	Value
Power, kW	10 kW/Port
Port Voltage (Grid/PV/Battery/Load) (V)	200/200/200/400
Core material	Ferrite, B: 0.25T
Litz wire	AWG 8
B_{max} (T)	0.20799
No. of Turns (Grid/PV/Battery /Load)	3/3/3/6
Leakage inductances (uH) (G/PV/ Bat. /Load)	2/2/2/2
Magnetizing Inductance (uH)	75
Core Losses (W)	22.96
Winding Losses (W)	20.67
Total Losses (W)	43.63
Efficiency (%)	99.56

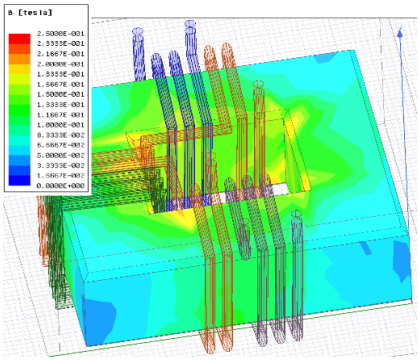

Fig. 4. Flux distribution of the designed four-port transformer

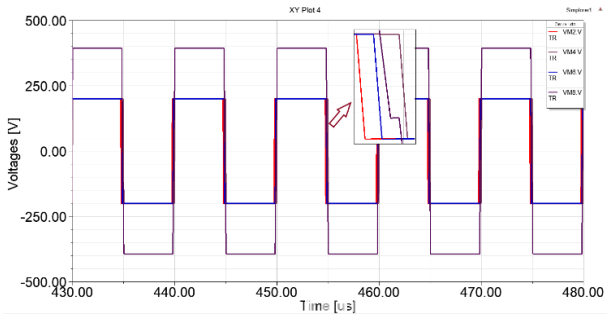

(a)

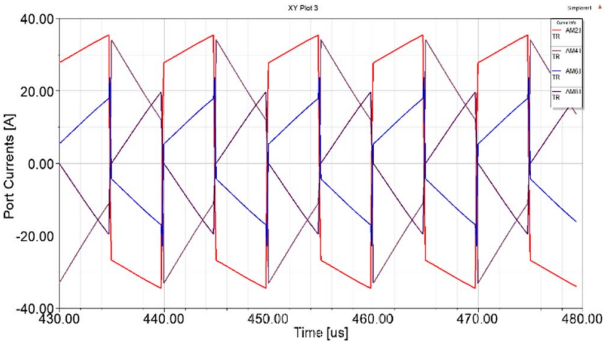

(b)

Fig. 5. Co-simulation results of the designed transformer, (a) Voltage waveforms, (b) Current waveforms

In this study, a four-port SST is proposed as depicted in Fig. 7. Here, L_1, L_2, L_3 and L_4 are the corresponding winding leakage inductances combined with external inductor. For simplicity, mutual-leakage inductances presented in [11] are not considered here. The power flow between any two ports is calculated by (1).

The equivalent circuit given in Fig. 8 can be obtained from Fig. 7. Here, L_m is magnetizing inductance; L_1 is port-1 leakage inductance; and L_2', L_3' and L_4' are leakage inductances of ports 2, 3 and 4, respectively, referred to port-1; v_1, v_2', v_3', v_4' and i_1, i_2', i_3', i_4' are port voltages and currents referred to port-1. It is clear from Fig. 8 and (1) that the equivalent inductances between the ports should be obtained to calculate the power flow. Thevenin equivalent circuit can be used for this purpose. The Thevenin equivalent circuit between port-x and port-y referred to port-1 is given in Fig. 9 (a) [7]. By neglecting the magnetization inductance,

the equivalent inductances between the ports can be written as (2)-(7):

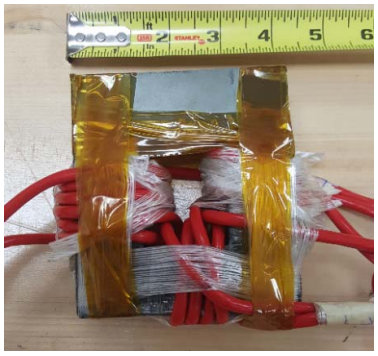

Fig. 6. Designed four-port MPSST prototype

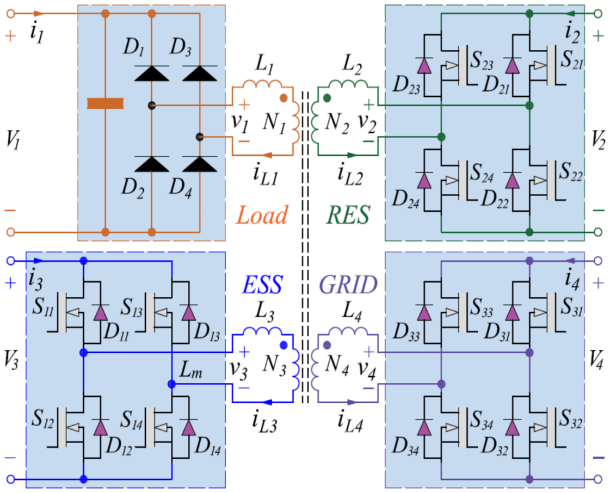

Fig. 7. Four-port SST circuit model.

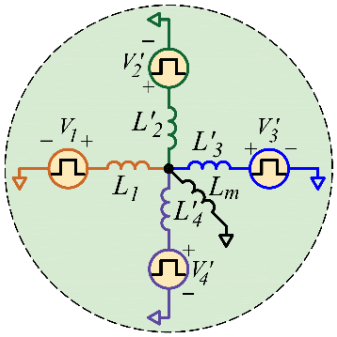

Fig. 8. Equivalent circuit of the four-port SST.

$$L_{12} = L_{21} = \frac{L_1L_3'L_4' + L_1L_2'L_4' + L_1L_2'L_3' + L_2'L_3'L_4'}{L_3'L_4'} \quad (2)$$

$$L_{13} = L_{31} = \frac{L_1L_3'L_4' + L_1L_2'L_4' + L_1L_2'L_3' + L_2'L_3'L_4'}{L_2'L_4'} \quad (3)$$

$$L_{14} = L_{41} = \frac{L_1L_3'L_4' + L_1L_2'L_4' + L_1L_2'L_3' + L_2'L_3'L_4'}{L_2'L_3'} \quad (4)$$

$$L_{23} = L_{32} = \frac{L_1L_3'L_4' + L_1L_2'L_4' + L_1L_2'L_3' + L_2'L_3'L_4'}{L_1L_4'} \quad (5)$$

$$L_{24} = L_{42} = \frac{L_1L_3'L_4' + L_1L_2'L_4' + L_1L_2'L_3' + L_2'L_3'L_4'}{L_1L_3'} \quad (6)$$

$$L_{34} = L_{43} = \frac{L_1L_3'L_4' + L_1L_2'L_4' + L_1L_2'L_3' + L_2'L_3'L_4'}{L_1L_2'} \quad (7)$$

Similarly, the Thevenin-equivalent voltages can be written for this circuitry. However, the Thevenin-equivalent voltage of a port is not the same for every power flow analysis. For instance, the Thevenin-equivalent voltage of port-3 is written in (8) and (9) when power flows from port-1 to port-3 and from port-2- to port-3, respectively.

$$v_{TH3_{1-3}} = \frac{L_2'L_4'}{L_2'L_3' + L_2'L_4' + L_3'L_4'} v_3' \quad (8)$$

$$v_{TH3_{2-3}} = \frac{L_1'L_4'}{L_1'L_3' + L_1'L_4' + L_3'L_4'} v_3' \quad (9)$$

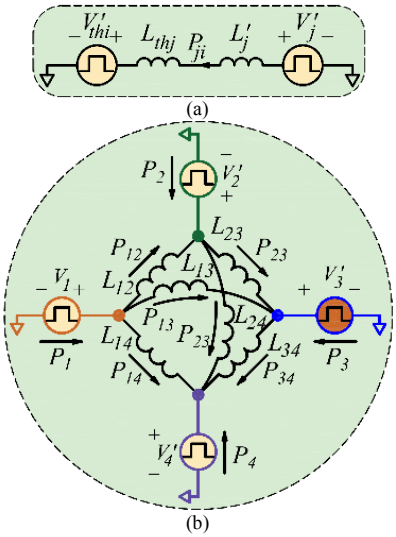

Fig. 9. The equivalent circuit of the four-port SST, a) Equivalent circuit for two ports, b) Equivalent circuit with equivalent inductances among the ports.

After obtaining all of the equivalent inductances between the ports, the equivalent circuits which is used to calculate the flowing power between the ports and total port power are calculated and drawn in Fig. 9 (b). According to current directions, the power equations for each port can be written as below:

$$P_2 = P_{12} - P_{23} - P_{24} \quad (10)$$

$$P_3 = P_{13} + P_{23} - P_{34} \quad (11)$$

$$P_4 = P_{14} + P_{24} + P_{34} \quad (12)$$

$$P_1 = -P_2 - P_3 - P_4 \quad (13)$$

Then, by using (1) and (10)-(13), power equations for each port can be obtained. For port-2, (14) can be written as:

$$P_2 = \frac{V_1 V_{TH2_{1-2}}}{2\pi^2 f_s L_{12}} \phi_2(\pi - \phi_2) - \frac{V_2 V_{TH3_{2-3}}}{2\pi^2 f_s L_{23}} (\phi_2 - \phi_3)(\pi - \phi_2 + \phi_3) - \frac{V_2 V_{TH4_{2-4}}}{2\pi^2 f_s L_{24}} (\phi_2 - \phi_4)(\pi - \phi_2 + \phi_4) \quad (14)$$

Power equations for the other ports can be written similarly. It can be seen that the power of each port depends on all of the phase angles of other ports. This makes the control of the system very complicated. To decouple the equations, a small gain (x+Δx) linearization method is applied to the power equations. If it is applied to (14), then power equation has two components P_x and ΔP_x as follows [17]:

$$P_2 + \Delta P_2 = \frac{V_1 V_{TH2_{1-2}}}{2\pi^2 f_s L_{12}}(\phi_2 + \Delta\phi_2)(\pi - \phi_2 - \Delta\phi_2) - \frac{V_2 V_{TH3_{2-3}}}{2\pi^2 f_s L_{23}}(\phi_2 + \Delta\phi_2 - \phi_3 - \Delta\phi_3)(\pi - \phi_2 - \Delta\phi_2 + \phi_3 + \Delta\phi_3) - \frac{V_2 V_{TH4_{2-4}}}{2\pi^2 f_s L_{24}}(\phi_2 + \Delta\phi_2 - \phi_4 - \Delta\phi_4)(\pi - \phi_2 - \Delta\phi_2 + \phi_4 + \Delta\phi_4) \quad (15)$$

Here, the power component P_x represents the operation point of the converter which depends on V_x, V_y , L_{xy}, V_x, ϕ_x, and ϕ_y, while ΔP_x component represents the power variation which depends on the variation of $\Delta\phi_x$, and $\Delta\phi_y$. This makes $\Delta\phi_x$ and $\Delta\phi_y$ perturbation control variables, and these perturbation variables can be used in control loop to control the power flow. Then, power variation components can be written as below:

$$\Delta P_2 = \frac{V_1 V_{TH2_{1-2}}}{2\pi^2 f_s L_{12}}(-2\phi_2 + \pi)\Delta\phi_2 - \frac{V_2 V_{TH3_{2-3}}}{2\pi^2 f_s L_{23}}(-2\phi_3 + 2\phi_2 + \pi)\Delta\phi_3 + \frac{V_2 V_{TH3_{2-3}}}{2\pi^2 f_s L_{23}}(-2\phi_3 + 2\phi_2 + \pi)\Delta\phi_2 \mathrm{b} - \frac{V_2 V_{TH4_{2-4}}}{2\pi^2 f_s L_{24}}(-2\phi_4 + 2\phi_2 + \pi)\Delta\phi_4 + \frac{V_2 V_{TH4_{2-4}}}{2\pi^2 f_s L_{24}}(-2\phi_4 + 2\phi_2 + \pi)\Delta\phi_2 \quad (16)$$

If ΔP_3 and ΔP_4 are obtained by using the same method, they can be written in a linear system equation form as below:

$$\begin{bmatrix}\Delta P_2 \\ \Delta P_3 \\ \Delta P_4\end{bmatrix} = \begin{bmatrix}(a+b+c) & -b & -c \\ -b & (b+d+e) & -e \\ -c & -e & (c+e+f)\end{bmatrix}\begin{bmatrix}\Delta\phi_2 \\ \Delta\phi_3 \\ \Delta\phi_4\end{bmatrix},$$

$$\Delta P = K \cdot \Delta\phi \quad (17)$$

where $a = \frac{V_1 V_{TH2_{1-2}}}{2\pi^2 f_s L_{12}}(-2\phi_2 + \pi)$, $b = \frac{V_2 V_{TH3_{2-3}}}{2\pi^2 f_s L_{23}}(-2\phi_3 + 2\phi_2 + \pi)$, c= $\frac{V_2 V_{TH4_{2-4}}}{2\pi^2 f_s L_{24}}(-2\phi_4 + 2\phi_2 + \pi)$, $d = \frac{V_1 V_{TH3_{1-3}}}{2\pi^2 f_s L_{13}}(-2\phi_3 + \pi)$, $e = \frac{V_2 V_{TH3_{2-3}}}{2\pi^2 f_s L_{23}}(-2\phi_3 + 2\phi_2 + \pi)$ and $f = \frac{V_1 V_{TH4_{1-4}}}{2\pi^2 f_s L_{14}}(-2\phi_4 + \pi)$.

The control variable can be calculated depending on the required power variations in accordance to (17).

$$\Delta\phi = K^{-1} \cdot \Delta P \quad (18)$$

As seen from (18), the power variation of any port only depends on its control variable, and thus decoupled power flow control is obtained.

IV. Experimental and Simulation Results

The proposed four-port SST and the control scheme is designed and validated through simulation and experimental results. The simulation results are carried out with MATLAB/Simulink. The control scheme is implemented on Altera FPGA board. The switching frequency is chosen to be 100 kHz. The proposed system is designed for distributed generation systems. It is assumed that the four-port SST ports are connected to: a renewable power source (e.g. PV modules), a battery energy storage system, a grid, and a load. Many different scenarios can be designed and implemented to provide better energy reliability or decrease the energy cost. However, these scenarios are not discussed here, and it is assumed that one energy management system provides current references to the system. Then, the performance of the proposed decoupled control scheme and the four-port SST is tested for these conditions. The renewable energy port is controlled to obtain maximum available power from the renewable source. Therefore, it is assumed that a MPPT controller provides a current reference for the renewable port. Similarly, it is assumed that a current reference is provided for the battery port. Then, the current reference of the grid port is generated by a PI controller, and the output voltage is kept at its desired value.

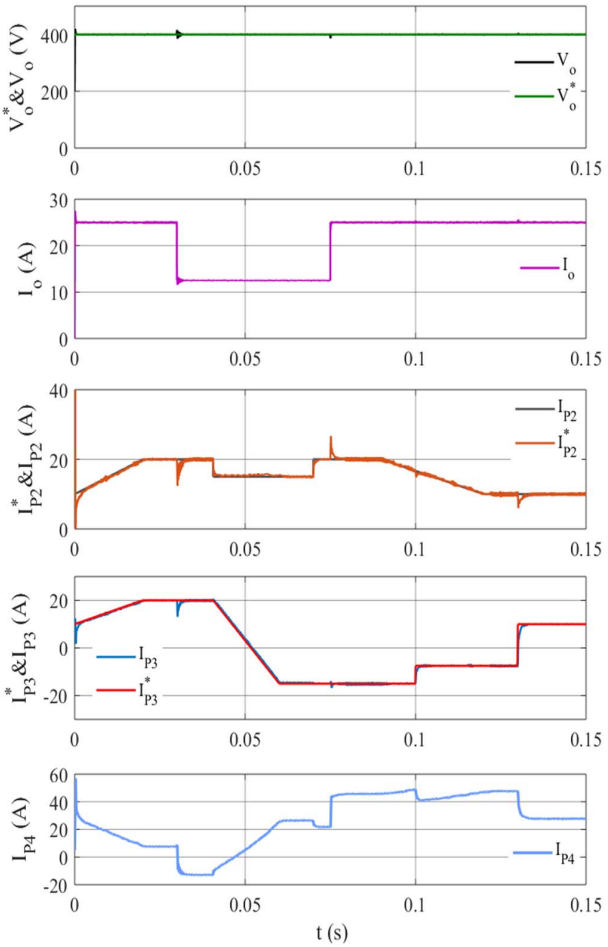

Fig. 10. Output voltage, output current and other port currents of the proposed four-port SST for different operation conditions.

In Fig. 10, the output voltage and its reference signal waveforms, output current waveform, Port-2 (PV port) current and its reference signal waveforms, Port-3 (Battery port) current and its reference signal waveforms, and Port-4 (Grid port) current waveform are given. As explained before, the reference currents for Port-2 and Port-3 are randomly determined and the reference current waveform for Port-4 is generated with the PI controller. After the variation of

reference signals are determined for Port-2 and Port-3 and a load change is applied, the performance of the proposed control scheme is tested. As seen from figure, the output voltage, Port-2 and Port-3 currents are tracking their reference signals and the performance of the proposed control of the proposed scheme is validated. It is seen that, proposed decoupled control scheme successfully tracks the reference signal for each port, and keeps the output voltage constant. It is also seen that it provides a good transient response.

The port currents waveforms of the four-port SST obtained from simulation and experimental studies are given in Fig. 11 and Fig. 12 for different operation conditions. In both figures, Port-2 is the most leading port; i.e., it provides more power to the other ports and load port. While Port-3 is the most lagging port in Fig. 11, the most lagging port is Port-4 in Fig. 12. The phase shift values are defined by (18) to track the power references of each port for any operation condition.

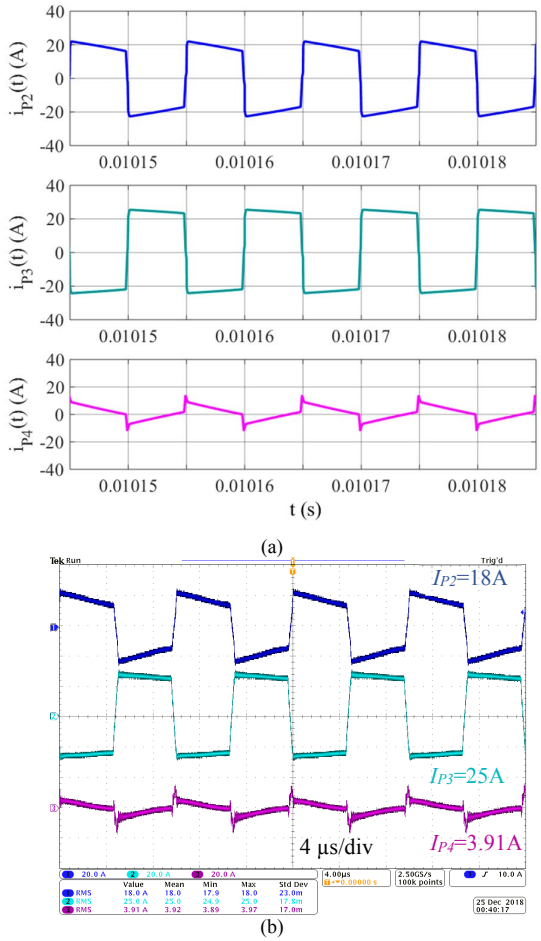

Fig. 11. Transformer winding currents: a) Simulation results, b) Experimental results (Ch. 1 is the most leading, Ch. 2 is the most lagging port.).

V. CONCLUSION

In this study, design of a four-port SST transformer and its decoupled control scheme is presented. The transformer includes two active bidirectional ports, one active unidirectional port, and one diode based unidirectional converter. The design details of the four-port transformer including core material selection, winding placement are investigated and validated with FEA simulations. The system is developed for fast, modular, and isolated utilization of DG and/or battery energy storage in the power system. The four-port SST is modelled and a control scheme is designed in order to control the power flow among the converter ports as well as ensure voltage regulation at the uncontrolled output port. In order to decouple the power sharing equations of the multiport system, a small signal linearization approach is applied to the power sharing equations. Simulation and experimental results have shown that the proposed system can control the power flow among the ports and the load port output voltage independently. It is seen that the proposed system provides a smooth control and power transfer between the ports as desired.

ACKNOWLEDGMENT

This material is based upon work supported by the National Science Foundation under Grant No. 1650470 for I/UCRC GRAPES center. Any opinions, findings, and conclusions or recommendations expressed in this material are those of the author(s) and do not necessarily reflect the views of the National Science Foundation. Dr. Necmi Altin and Dr. Saban Ozdemir thank the financial support, which they have received from the

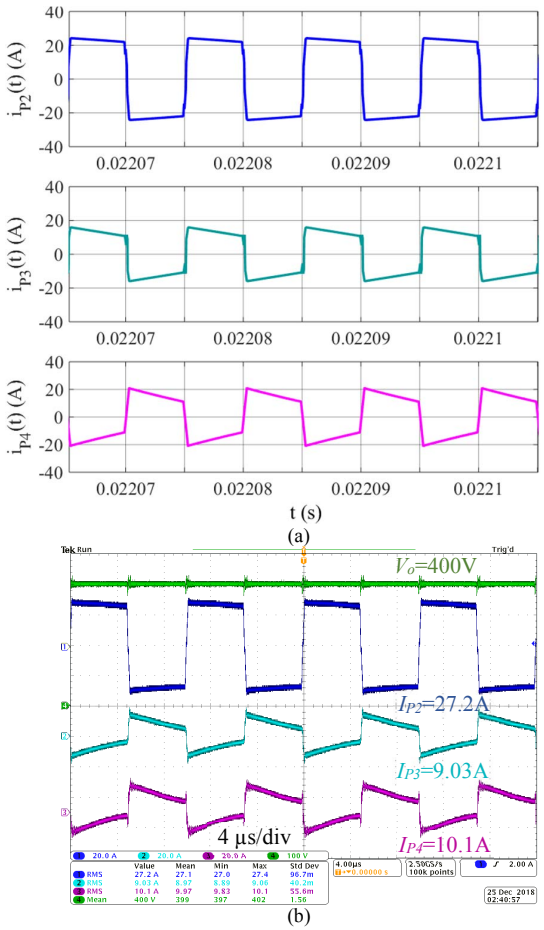

Fig. 12. The transformer winding currents, a) Simulation results, b) Experimental results (Ch. 1 is the most leading, Ch. 3 is the most lagging port.).

Scientific and Technological Research Council of Turkey (TUBITAK) BIDEB-2219 Postdoctoral Research program.

REFERENCES

[1] M. Rashidi, A. Bani-Ahmed, R. Nasiri, A. Mazaheri, A. Nasiri, "Design and implementation of a multi winding high frequency transformer for MPSST application", IEEE 6th International Conference on Renewable Energy Research and Applications (ICRERA), pp.491-494, 5-8 Nov. 2017.

[2] T. Guillod, F. Krismer, R. Färber, C. M. Franck and J. W. Kolar, "Protection of MV/LV solid-state transformers in the distribution grid", IECON 2015-41st Annual Conference of the IEEE Industrial Electronics Society, Yokohama, pp. 3531-3538, 2015.

[3] S. Ozdemir, S. Balci, N. Altin and I. Sefa, I., "Design and performance analysis of the three-level isolated DC-DC converter with the nanocyrstalline core transformer", International Journal of Hydrogen Energy, vol.42, no.28, pp.17801-17812, 2017.

[4] M. Rashidi, A. Nasiri and R. Cuzner, "Application of multi-port solid state transformers for microgrid-based distribution systems," 2016 IEEE International Conference on Renewable Energy Research and Applications (ICRERA), Birmingham, pp. 605-610, 2016.

[5] B. Zhou and T. Littler, "Local storage meet local demand: a technical solution to future power distribution system", IET Generation, Transmission & Distribution, vol. 10, no. 3, pp. 704-711, 2016.

[6] K. Li, Z. Zhao, L. Yuan, C. Zhang, W. Wen and J. Sun, "Synergetic Control of High-Frequency-Link Based Multi-Port Solid State Transformer," 2018 IEEE Energy Conversion Congress and Exposition (ECCE), Portland, OR, 2018, pp. 5630-5635.

[7] S. Falcones, R. Ayyanar and X. Mao, "A DC-DC multiport-converter-based solid-state transformer integrating distributed generation and storage", IEEE Transactions on Power Electronics, vol. 28, no. 5, pp. 2192-2203, May 2013.

[8] C. Gu, Z. Zheng, L. Xu, K. Wang and Y. Li, "Modeling and control of a multiport power electronic transformer (PET) for electric traction applications", IEEE Transactions on Power Electronics, vol. 31, no. 2, pp. 915-927, Feb. 2016.

[9] J. W. Kolar and G. Ortiz, "Solid state transformer concepts in traction and smart grid applications" 28th Applied Power Electronics Conference and Exposition (APEC 2013), 2013.

[10] L. Wang, Z. Wang, and H. Li, "Asymmetrical duty cycle control and decoupled power flow design of a three-port bidirectional DC-DC converter for fuel cell vehicle application," IEEE Transactions on Power Electronics, vol. 27, no. 2, pp. 891-904, Feb. 2012.

[11] D. Liu and H. Li, "A ZVS bi-directional DC–DC converter for multiple energy storage elements", IEEE Transactions on Power Electronics, vol. 21, no. 5, pp.1513-1517, 2006.

[12] Y. Tran, F. D. Freijedo and D. Dujic, "Open-Loop Power Sharing of Three-Port DC-DC Resonant Converters," 2019 IEEE Applied Power Electronics Conference and Exposition (APEC), Anaheim, CA, USA, 2019, pp. 2138-2144.

[13] S. Roy, A. De and S. Bhattacharya, "Multi-port solid state transformer for inter-grid power flow control," 2014 International Power Electronics Conference (IPEC-Hiroshima 2014 - ECCE ASIA), Hiroshima, 2014, pp. 3286-3291.

[14] V. N. S. R. Jakka and A. Shukla, "A triple port active bridge converter based multi-fed power electronic transformer," 2016 IEEE Energy Conversion Congress and Exposition (ECCE), Milwaukee, WI, 2016, pp. 1-8.

[15] S. Baek and S. Bhattacharya, "Isolation Transformer for 3-Port 3-Phase Dual-Active Bridge Converters in Medium Voltage Level," in IEEE Access, vol. 7, pp. 19678-19687, 2019.

[16] S. Balci, I. Sefa, and N. Altin. "An investigation of ferrite and nanocrystalline core materials for medium-frequency power transformers," Journal of Electronic Materials, vol. 45, no. 8, pp. 3811-3821.

[17] M. Grabarek, M. Parchomiuk and R. Strzelecki, "Conjugated control of triple active bridge converter with common HFT", 2017 11th IEEE International Conference on Compatibility, Power Electronics and Power Engineering (CPE-POWERENG), 4-6 April 2017.